Investigating the influence of sheared currents on ship hydrodynamics in confined water using Computational Fluid Dynamics

Momchil Terziev*, Tahsin Tezdogan†, Atilla Incecik* and Claire De Marco Muscat-Fenech‡

*Faculty of Engineering, University of Strathclyde, Glasgow, UK
† Department of Naval Architecture, Ocean and Marine Engineering, University of Strathclyde, Glasgow, UK
‡Faculty of Engineering, University of Malta, Msida, Malta

Email: (MT) momchil.terziev@strath.ac.uk
Web page : (MT) https://pureportal.strath.ac.uk/en/persons/momchil-terziev

ABSTRACT

The field of ship hydrodynamics in confined water has received increased attention by the academic community in recent years. Nevertheless, a number of phenomena occurring in confined waters are yet to be examined using high fidelity Computational Fluid Dynamics (CFD) or experimentally. One particular case is the presence of sheared currents and their impact on the performance of a ship. Such currents can be generated in confined waters as a result of the natural flow of water in rivers or due to the action of tidal influences in long canals. Alternatively, due to the short fetch of many inland waterways, the action of wind may result in the production of a sheared current. This work aims to investigate these effects by making use of a commercially available Reynolds Averaged Navier-Stokes (RANS) solver. A number of current profiles are numerically modelled to determine their influence on ship performance and the manner in which ship waves interact with the background current. The present study will contribute to the understanding of restricted water effects by revealing the impact of shear currents on ship performance.

1. Introduction

The study of ship resistance is a rich and diverse field, comprising a multitude of methods and approaches. In recent years, Reynolds Averaged Navier-Stokes (RANS) methods have emerged as the dominant approach in the field. Virtually every conceivable aspect of numerical ship resistance prediction has been investigated (De Luca et al., 2016; Elsherbiny et al., 2019; Kok et al., 2020; Mucha et al., 2016; Song et al., 2019; Terziev et al., 2019; Tezdogan et al., 2016). However, to the best of the authors' knowledge, numerical investigations of the effect of a sheared current on ship performance has yet to be conducted. From a physical point of view, this is a highly relevant phenomenon that may occur in an open sea, in shallow, or confined waters. In the former case a current might form due to a variety of reasons, such as the presence of wind, density and temperature variations in the water, or tidal influences. For shallow water cases, Ellingsen (2014) derived a theoretical framework for investigating the effects of a depth varying current on ship waves. Such a current can form a boundary layer when it is driven by tidal forces, or alternatively, an approximately linear velocity profile might form resulting due to the action of wind forces (Kirby and Chen, 1989). This paper aims to investigate the effects of sheared currents on ship performance using a commercially available RANS solver, Star-CCM+, version 15.02.007. To begin with, results are compared against the experimental results of Elsherbiny et al. (2019) for a rectangular canal to build confidence in the approach. Subsequently, cases are examined including different profiles and strengths of the depth-varying current. The results are quantified in terms of the wave elevation and resistance encountered by the ship in each case. The purpose of this work is to lay the foundations onto which a larger, more in-depth study can be built.

2. Background

Although investigations of sheared current effects on ship hydrodynamics has not been studied with a numerical solver previously, a large body of literature exists on the theoretical aspects of the problem (Chen and Zou, 2019; Chen et al., 2019; Jonsson et al., 1978; Maïssa et al., 2016, 2013; Skop, 1987; Swan and James, 2000; Trulsen and Mei, 1993). These investigations vary from analytical (Jonsson et al., 1978; Kantardgi, 1995; Peregrine, 1976; Swan and James, 2000) to approximate (Kirby and Chen, 1989; Skop, 1987). Recently, the effects of a depth varying current were extended to the study of ship wave resistance (Li et al., 2019; Li and Ellingsen, 2016). Additionally, experimental studies on the waves shed from a cylindrical structure have also been investigated (Chen et al., 2019), while numerical solutions of wave-current interactions were presented by Markus et al. (2013) and Zhang et al. (2014). However, ship wave making is more complex due to the possibility of interference between different components of the wave system (He et al., 2015; Noblesse et al., 2014). This work will attempt to bridge this gap.

To characterise the shear current, the notation of Ellingsen and Brevik (2014) is adopted. Specifically, Eq. (1) and Eq. (2) determine the strength and shape of the shear current:

$$U(z) = U_0 + Sz \quad (1)$$

$$S = U_0/h \quad (2)$$

where S is the vorticity, since its units are s^{-1}, z is the local depth with $z = -h$ at the seabed and $z = 0$ at the undisturbed free surface where the sheared current causes the water to move with a speed equal to U_0, while the depth varying current is $U(z)$. A case where the flow varies in the vertical (z) direction according to Eq. (1) is hereafter referred to as the "constant vorticity" case, reflecting the constant value of S.

3. Case studies

Physical values of S are difficult to estimate. Therefore, focus is shifted from defining S as a variable to defining U_0, and predicting S as a function of a constant water depth, h, and an assumed U_0. To produce a range of values, U_0 is varied from 0% to 30% of the ship speed in intervals of 10%. These current velocities are initially applied to the canal case investigated experimentally by Elsherbiny et al. (2019). Namely, the canal has a width of 4.6m and a depth of 0.32m, therefore, $h = 0.32$m in Eq. (2). The well-known KRISO containership (KCS), with a scale factor of 1:75, whose principal characteristics are shown in Table 1, advances through this canal. In the present study, the KCS speed is limited to a depth Froude number, F_h, ($F_h = U_{ship}/\sqrt{gh}$) of 0.57 (U =1.001 m/s), although future work will incorporate a greater number of ship speeds.

Table 1. Principal dimensions of the KCS model and canal.

Quantity	Symbol	Value	Unit
Length	L	3.067	m
Beam	B	0.429	m
Draught	T	0.144	m
Water depth	h	0.32	m
Canal width	w	4.6	m

To investigate the impact of the depth-varying current's profile, additional case studies to the canal mentioned previously are modelled. Firstly, the computational domain is expanded in the lateral (y) direction to reach two ship lengths wide in the port and starboard directions while preserving an identical mesh set-up. As shown subsequently, the sheared current interacts strongly with the canal sides. Thus, it is instructive to examine a shallow sea case and observe the differences in the flow. To this case, a $1/7^{th}$ power law-shaped current velocity profile is applied using the same U_0 values, namely $U_0 = 0$, 10%, 20%, and 30% of the ship speed. In cases where currents are created by tidal influences, such velocity profiles are more

likely to be realistic. The equation describing this 1/7th power law profile is given in Eq. (3), where d is the wall distance ($d = 0$ m on the canal bottom and side).

$$U(z) = U_0 \times (d/h)^{1/7} \quad (3)$$

Therefore, the water flows with identical speeds on the water surface in each case, allowing an assessment of the depth-varying velocity profile influence on ship resistance and wave making.

4. Numerical set-up

All numerical simulations are performed using the commercially available RANS solver, Star-CCM+, version 15.02.007. Following Terziev et al. (2019), the k-ω Wilcox turbulence model is used due to its computational efficiency and accuracy (Wilcox, 2006). All discretisation terms are set to 2nd order accuracy. Time is advanced by $0.3h_x/U_{ship}$, where h_x is the mesh dimension on the finest part of the free surface. This ensures the Courant number criterion of (<0.5) is satisfied everywhere in the domain. A high y^+ strategy is employed, with values of 100~150 in all simulations.

The computational mesh is generated within the automatic facilities of Star-CCM+. Refinements are set at the free surface, ship, bow and stern regions, and kelvin wedge. The resulting mesh numbers feature 2,386,928 cells for the canal case study, and 3,176,433 for the wider, shallow sea case. The discretisation uncertainty of an example case is estimated in Section 6. It should be noted that mesh numbers are not altered when including a sheared current. The computational domain dimensions, including the boundary conditions are shown in Figure 1, while the generated mesh is depicted in Figure 2 for the canal case.

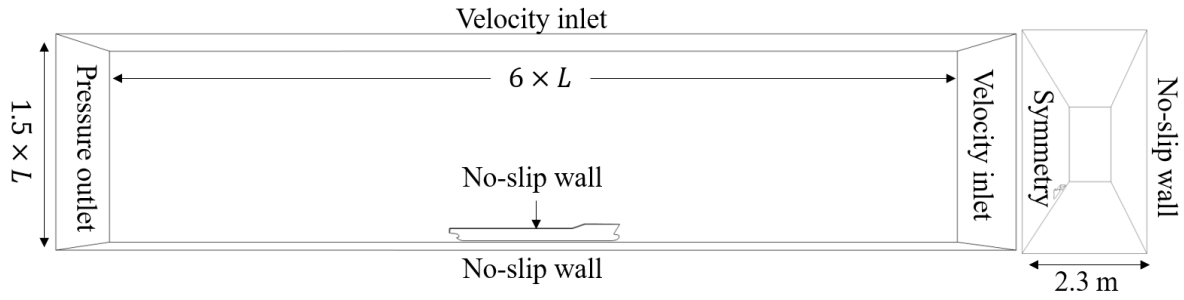

Figure 1. Computational domain and boundary conditions, $L = 3.067$ m is the ship length.

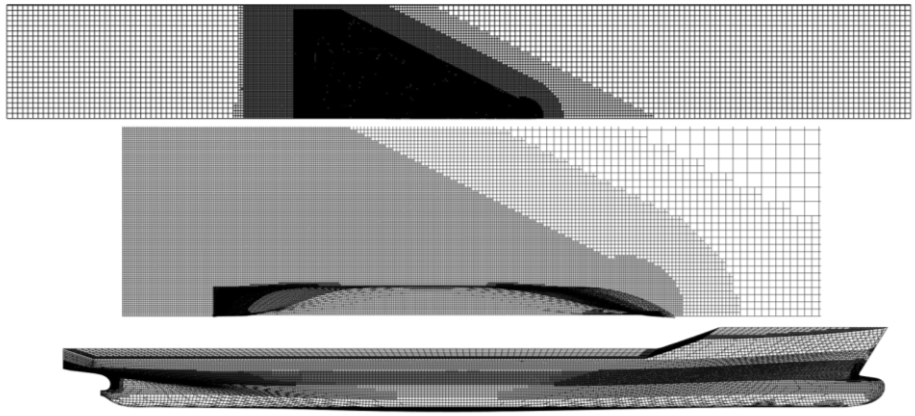

Figure 2. Generated mesh within the automatic facilities of Star-CCM+. Top: a full domain top view of the mesh on the water surface; middle: a zoom in on the mesh near the ship; bottom: mesh on the ship hull. It should be noted that the mesh characteristics do not change when studying different sheared currents.

To model the fluid flow, a planar motion mechanism approach is adopted. The entire computational domain is translated in space with the speed of the ship. In the $U_0 = 0$ case, the inlet boundary has a zero inflow and the ship moves over a static fluid, which is adjusted

according to the case study. Doing so allows the sheared current to be introduced independently of the ship velocity. The canal side and bottom are assigned a flow velocity equal to the combined flow in the opposite direction of the ship motion to prevent any relative motions between wall boundaries and the flow. Thus, in the global coordinate system, the ship moves over static fluid and sides/canal bottom. However, this cannot be achieved in the sheared current cases where a canal is investigated because the combined flow speed varies across the side boundary in the z direction. The impact of this is examined in the following section. It should be noted that sinkage and trim are not accounted for in this work.

5. Results and discussion

To begin with, the predicted resistance is compared from all case studies. A comparison is depicted in Figure 3. Here, the resistance is given in Newtons instead of in coefficient form, since it is not clear what velocity should be used in making the data dimensionless. The result for the canal (4.49 N) at $U_0 = 0$ (no current) is 0.244% lower than the experimental value reported by Elsherbiny et al. (2019) of approximately 4.50 N. On the other hand, the resistance of the ship in the wide sea case is 9.68% lower than the experiment. This highlights the importance of side wall effects. Hereafter, the simulations are considered of sufficient accuracy for the purpose of this work.

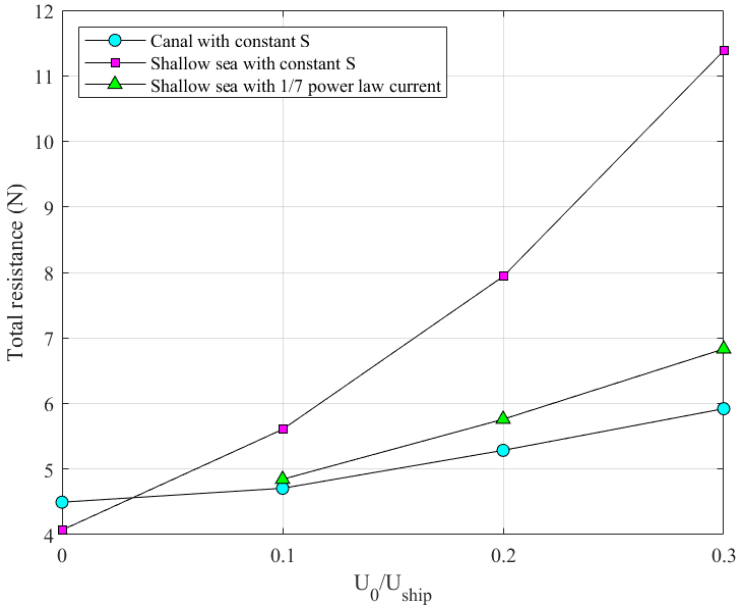

Figure 3. Total resistance comparison for all case studies.

Figure 3 demonstrates the importance of the shape of the current on ship resistance. The results for a canal with a current of constant vorticity, S, (Eq. (1) and Eq. (2)) exhibit the lowest resistance. The side wall effect is seen for $U_0/U_{ship} = 0$. As U_0/U_{ship} attains values higher than 0, the canal case shows the least resistance, partly due to the omission of sinkage and trim.

As shown in Figure 4, the flow is affected by the presence of the ship, marked by the local depression near the canal side. As the shear current intensifies, this influence is magnified, creating waves that interact with the primary wave system of the ship. The Kelvin wake of the ship is also modified noticeably by the presence of the current. The case where $U_0 = 0$, the waves resemble the well-known shape, however, the diverging wave system appears to be supressed by the current at $U_0 = 0.3U_{ship}$.

The depression characterising the near field disturbance is stronger in the presence of a shear current, which is depicted in Figure 4. Therefore, the ship is likely to experience a greater sinkage and/or trim. If this was accounted for, it may compensate partly for the observed difference in resistance values, reported in Figure 3.

The dynamic pressure distribution on the ship hull for these cases is depicted in Figure 5, where it is apparent that as the sheared current effect influence becomes stronger, the dynamic pressure increases. The aforementioned effect is particularly pronounced at the bow of the ship.

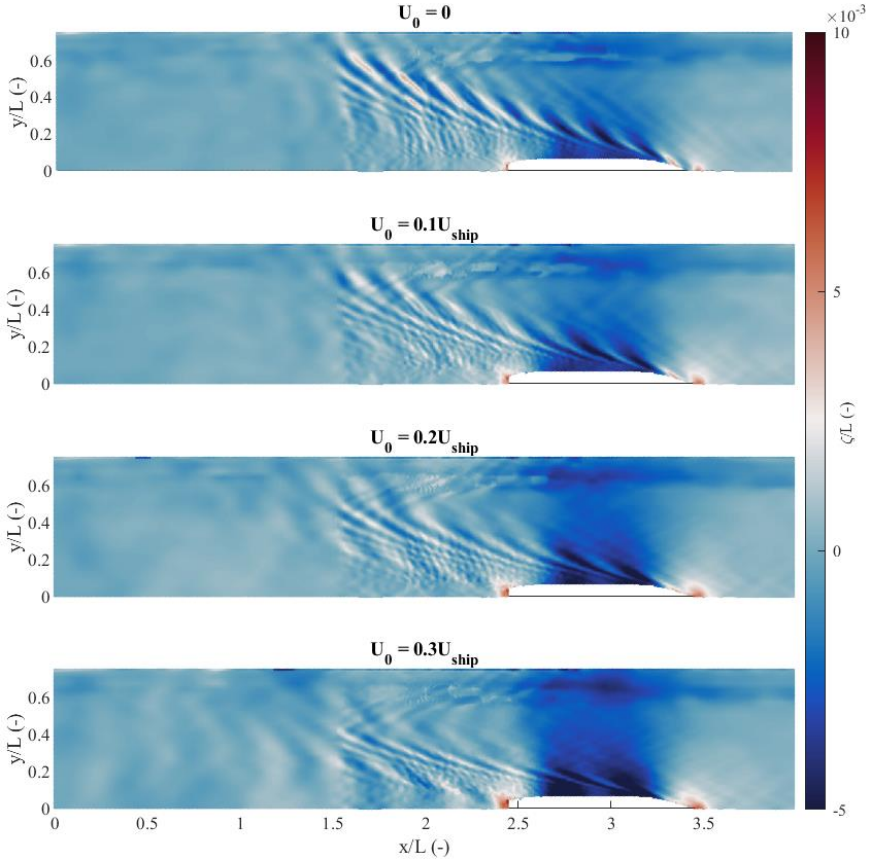

Figure 4. Effects of shear flow on ship-generated waves in a canal (constant vorticity only).

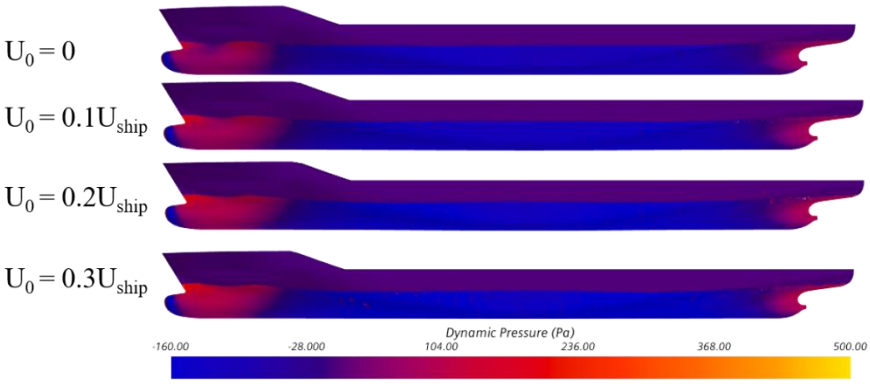

Figure 5. Dynamic pressure distribution on the ship advancing through the canal investigated by Elsherbiny et al. (2019) (4.6m wide and 0.32m deep). The current strength increases from 0 (top) to 30% of the ship speed (bottom).

In the shallow sea cases, the resistance curve for the sheared current depicts a non-linear increase with changes in U_0 when S is constant. However, when the current profile is that of a 1/7 power law, the increase in resistance is approximately linear. At the highest U_0, the resistance experienced by the ship when subjected to a 1/7 power law shape current is almost half that of the linear case (constant S).

The generated free surface disturbances are shown in Figure 6, where the linear and 1/7 variants of the current are compared. Here, the flow velocity of the water at the surface is the same in each column of the plot. Nevertheless, the differences within each column are clearly noticeable. In the case of constant S (linear current), the divergent wave system is initially supressed. However, at $U_0 = 0.3U_{ship}$, the divergent waves dominate the domain up to about

1.5 ship lengths in the y direction. At the same U_0 condition, the 1/7 power law current has suppressed the divergent wave system. The only difference between these two cases is the shape of the current in the z direction, i.e. as the seabed is approached.

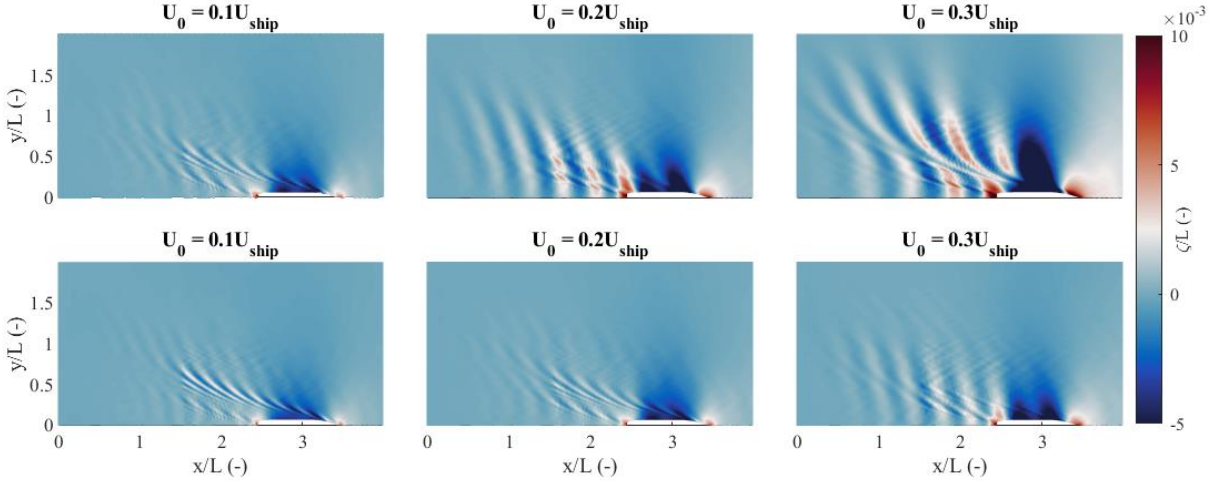

Figure 6. Effects of shear flow on ship-generated waves in a wide sea. Top: constant vorticity; bottom: 1/7th power law velocity distribution.

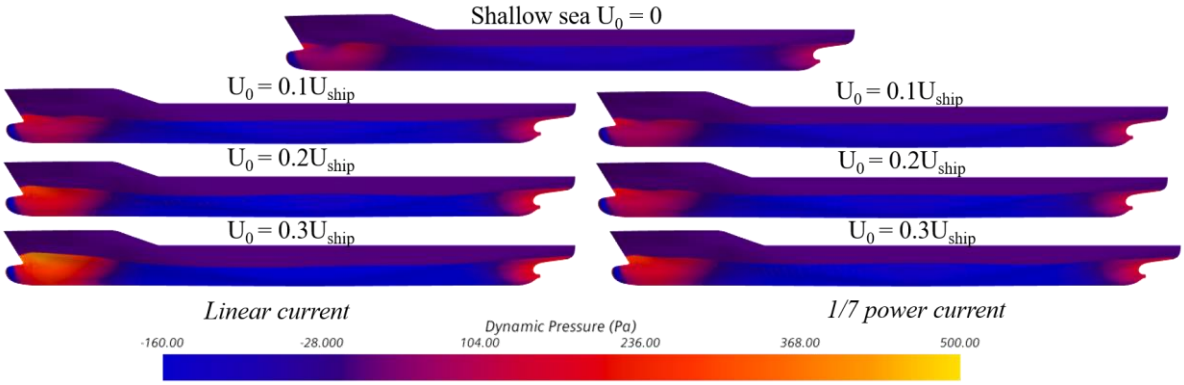

Figure 7. Dynamic pressure distribution on the ship advancing through a shallow sea. Right: linear current (constant vorticity); left: 1/7 power current (Eq. (3)).

Figure 7 depicts the dynamic pressure on the hull in the shallow sea cases. It is evident that a more uniform flow (the 1/7th power law shape) causes a lower pressure peak at the bow, explaining the differences in the wave field. However, it is important to examine why the divergent wave component of the constant vorticity case was supressed in the canal. For this reason, Figure 8 is constructed to show the effect of the shear current on the side boundaries. Figure 8 shows the shear current interaction with the side wall has created a vortex by the time the water reaches the ship. Once this happens, the near field pressure field of the ship pulls the vortex towards the centre of the canal, splitting it into two parts. A top view of this phenomenon and the resulting dynamic pressure at the canal bottom is depicted in Figure 9. Figure 9 demonstrates the vortex and boundary layer formed as a result of the sheared current at the canal side is pulled into the wavefield and interferes with the divergent part of the wave system, modifying it. This explains why the constant vorticity sheared current suppressed ship waves in the canal, but magnified them in an open shallow sea. In the latter case, there is no vortex formation to interfere and constrict the propagation of waves.

Once the flow passes into the coarse region of the domain aft of the ship (consult Figure 2), the boundary layer and vortex begin forming anew. A factor in this is that waves are practically eliminated due to the coarsening of the mesh. The boundary separating these two regions (waves resolved and waves unresolved due to mesh size) is clearly visible both in the wave field, as well as the dynamic pressure scar left on the canal bottom as a result of the vortex

splitting mentioned earlier and shown in Figure 9. The same phenomenon is observed in Figure 10 for the case $U_0 = 0.3U_{ship}$.

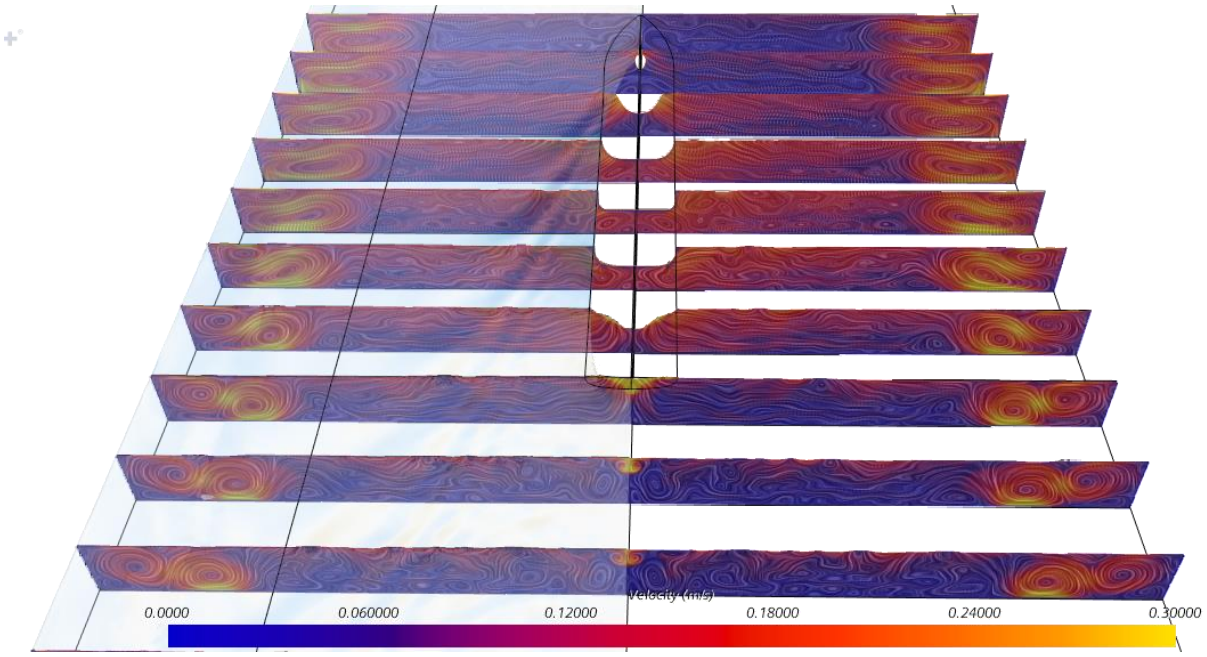

Figure 8. Shear current effects on the fluid flow around the ship sailing in a canal and subjected to $U_0/U_{ship} = 0.1$. Left: also includes the free surface. Note the velocity at the water surface due to the current is approximately 0.1 m/s.

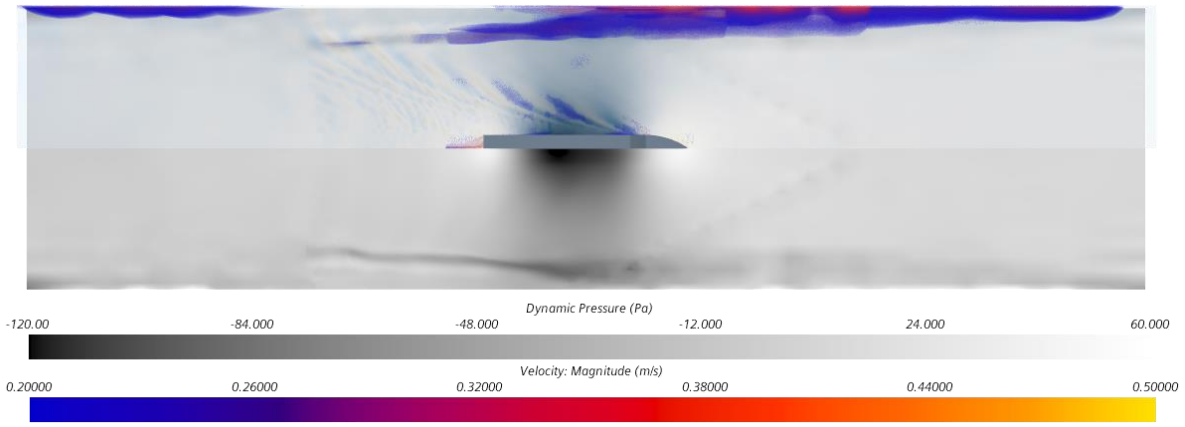

Figure 9. Dynamic pressure on the canal bottom and velocity of the fluid relative to the earth-fixed coordinate system. The top half of the figure contains the ship geometry, free surface and the velocity distribution in the range 0.2-0.5 m/s. Case depicted: $U_0/U_{ship} = 0.1$.

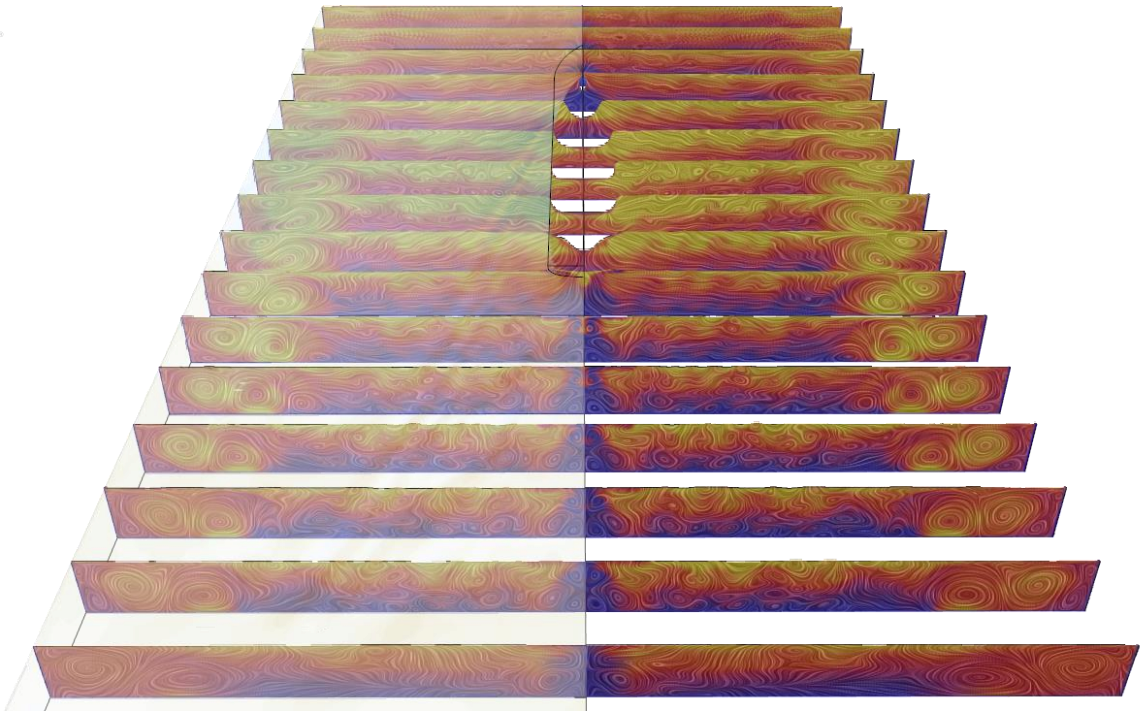

Figure 10. Shear current effects on the fluid flow around the ship sailing in a canal and subjected to $U_0/U_{ship} = 0.3$. Left: also includes the free surface. Note the velocity at the water surface due to the current is approximately 0.3 m/s; colour bar is the same as in Figure 8 (0 to 0.3 m/s).

Figure 10 demonstrates the effect of the current on ship wave disturbance in terms of velocity. Ship-generated waves modify the flow considerably when compared to the region upstream of the ship. Additionally, the aforementioned vortices block the wave field from extending toward the sides of the canal. This blockage is also responsible for an elevated flow velocity in the region adjacent to the ship, causing the waves to be swept downstream faster than would otherwise be the case. Although this phenomenon is largely restricted to the upper layers of the water column, wave effects decay exponentially with depth.

Shallow water waves typically extend their influence to the seabed, however, at $F_h = 0.57$, the deviation in the dispersion relation of shallow water waves from their deep water counterparts is less than 1% (Caplier et al., 2016). Therefore, the exponential decay with depth holds largely true in this case, and is predominantly the reason for the observed changes.

On the other hand, when the current follows a 1/7 power law shape, the changes in the upper parts of the water column in terms of velocity distribution are small. Hence, the net effect of the current is mostly that of an increase in the depth Froude number. If this reasoning is followed, the waves shown for $U_0/U_{ship} = 0.3$ for the shallow sea case are representative of those of $F_h \approx 0.74$ (if the flow velocity at the water surface is assumed to be representative). However, if one compares deep and shallow water dispersion characteristics in this case, the errors will be closer to 10% at this depth Froude number (Caplier et al., 2016). Therefore, the change in velocity profile exerts influence on the behaviour of the wave system, explaining the differences.

6. Discretisation uncertainty

In this section, the discretisation uncertainty is estimated for an example case. This is necessary to understand what confidence interval one can place in the numerical solution. To accomplish this, the Grid Convergence Method (GCI) is used, as described by Celik et al. (2008). Although the relations used to produce the overall uncertainty are omitted in this work, the reader is referred to the openly available literature for the derivation of each term (ASME (American Society of Mechanical Engineers), 2009; ITTC, 2008; Roache, 2016).

The main output from an discretisation uncertainty assessment is a symmetrical band around the fine solution to indicate the 95% confidence interval. This uncertainty stems from the mapping of the continuous governing equation onto a discrete set of points (Terziev et al.,

2020a). To estimate the uncertainty, one magnifies the fine grid size by a (in this case) constant factor, equal to $\sqrt{2}$ (ITTC, 2017), twice to produce a medium and coarse solution. The results from the uncertainty assessment are given in Table 2. The uncertainty assessment shows that an oscillatory behaviour is reproduced as the grid size changes. Nevertheless, the overall uncertainty according to the GCI method is $\pm$ 0.0029 N, or 0.064% of the fine solution, which is negligible.

Table 2. Results from the uncertainty assessment

Quantity	Value	Units
Refinement ratio	$\sqrt{2}$	-
Fine simulation resistance	4.4947	N
Medium simulation resistance	4.2663	N
Coarse simulation resistance	4.5054	N
GCI uncertainty	0.064% or $\pm$ 0.0029 N	-

The medium and coarse solutions featured 960,453 and 398,140 cells, respectively. To ensure this assessment is carried out adequately, the Courant number and aspect ratios of the grid must remain constant (Salas, 2006; Salas and Atkins, 2009). Therefore, the time-step is adjusted accordingly, according to the rule mentioned in previous sections of this paper. Namely, in all simulations, the Courant number is equal to 0.3 in the vicinity of the ship.

7. Conclusions and future work

This paper presented a useful starting point for further investigations into sheared current effects on ship hydrodynamics. It was demonstrated that the presence of such a current modifies ship-generated waves in unexpected ways. In a canal, a sheared current supressed divergent waves by forming a boundary layer on the canal side, blocking the propagation of the wave system away from the ship, and accelerating the near-surface flow in the vicinity of the ship. This caused waves to be swept downstream at a faster rate, thereby limiting their formation.

When a ship advances through a shallow sea with a shear current, the effect is different. The top layers of the water column are swept downstream faster, causing the waves to stretch reinforcing the divergent wave system in particular. The phenomenon causes a non-linear increase in the resistance of a ship. It was demonstrated that a ship's resistance advancing against a shear current of constant vorticity can be approximately double that of a ship advancing in a shear current in the form of a 1/7 power law.

The present study also showed that high predictive accuracy in terms of resistance can be achieved when comparing CFD to experimental results. It was found that an error in the region of 0.24% when considering the canal case study can be obtained. On the other hand, the resistance is 9.68% lower in a wide shallow sea than the canal case, highlighting the importance of considering side wall effects on ship performance.

This study can be extended in a variety of ways, including incorporating additional cases in the prediction of the discretisation uncertainty. Additionally, different shapes of current can be modelled in shallow and in deep waters to study their effects.

Acknowledgements

Results were obtained using the ARCHIE-WeSt High Performance Computer (www.archie-west.ac.uk) based at the University of Strathclyde. The authors gratefully acknowledge that the research presented in this paper was carried out as part of the EU funded H2020 project, VENTuRE (grant no. 856887). Figure 4 and Figure 6 in this paper were created using the cmocean package of perceptually uniform colourmaps, developed by Thyng et al. (2016).

References

ASME (American Society of Mechanical Engineers), 2009. Standard for Verification and

Validation in Computational Fluid Dynamics and Heat Transfer - ASME V&V 20-2009, ASME International.
Caplier, C., Rousseaux, G., Calluaud, D., David, L., 2016. Energy distribution in shallow water ship wakes from a spectral analysis of the wave field. Phys. Fluids 28. https://doi.org/10.1063/1.4964923
Celik, I.B., Ghia, U., Roache, P.J., Freitas, C.., 2008. Procedure for Estimation and Reporting of Uncertainty Due to Discretization in CFD Applications. J. Fluids Eng. 130, 078001. https://doi.org/10.1115/1.2960953
Chen, H., Zou, Q., 2019. Effects of following and opposing vertical current shear on nonlinear wave interactions. Appl. Ocean Res. 89, 23–35. https://doi.org/10.1016/j.apor.2019.04.001
Chen, L.F., Stagonas, D., Santo, H., Buldakov, E. V., Simons, R.R., Taylor, P.H., Zang, J., 2019. Numerical modelling of interactions of waves and sheared currents with a surface piercing vertical cylinder. Coast. Eng. 145, 65–83. https://doi.org/10.1016/j.coastaleng.2019.01.001
De Luca, F., Mancini, S., Miranda, S., Pensa, C., 2016. An Extended Verification and Validation Study of CFD Simulations for Planing Hulls. J. Sh. Res. 60, 101–118. https://doi.org/10.5957/josr.60.2.160010
Ellingsen, S., 2014. Ship waves in the presence of uniform vorticity. J. Fluid Mech. 742, 1–11. https://doi.org/10.1017/jfm.2014.28
Ellingsen, S., Brevik, I., 2014. How linear surface waves are affected by a current with constant vorticity. Eur. J. Phys. 35. https://doi.org/10.1088/0143-0807/35/2/025005
Elsherbiny, K., Tezdogan, T., Kotb, M., Incecik, A., Day, S., 2019. Experimental analysis of the squat of ships advancing through the New Suez Canal. Ocean Eng. 178, 331–344. https://doi.org/10.1016/j.oceaneng.2019.02.078
Gomit, G., Rousseaux, G., Chatellier, L., Calluaud, D., David, L., 2014. Spectral analysis of ship waves in deep water from accurate measurements of the free surface elevation by optical methods. Phys. Fluids 26. https://doi.org/10.1063/1.4902415
He, J., Zhang, C., Zhu, Y., Wu, H., Yang, C.J., Noblesse, F., Gu, X., Li, W., 2015. Comparison of three simple models of Kelvin's ship wake. Eur. J. Mech. B/Fluids 49, 12–19. https://doi.org/10.1016/j.euromechflu.2014.07.006
ITTC, 2017. ITTC-Recommended Procedures and Guidelines Uncertainty Analysis, Instrument Cali-bration ITTC Quality System Manual Recommended Procedures and Guidelines Procedure.
ITTC, 2008. Uncertainty Analysis in CFD Verification and Validation Methodology and Procedures. 25th ITTC 2008, Resist. Comm. 12.
Jonsson, I.G., Brink-Kjaer, O., Thomas, G.P., 1978. Wave action and set-down for waves on a shear current. J. Fluid Mech. 87, 401–416. https://doi.org/10.1017/S0022112078001688
Kantardgi, I., 1995. Effect of depth current profile on wave parameters. Coast. Eng. 26, 195–206. https://doi.org/10.1016/0378-3839(95)00021-6
Kirby, J.T., Chen, T.-M., 1989. Surface waves on vertically sheared flows: approximate dispersion relations. J. Geophys. Res. 94, 1013–1027.
Kok, Z., Duffy, J., Chai, S., Jin, Y., 2020. Multiple Approaches to Numerical Modeling of Container Ship Squat in Confined Water. J. Waterw. Port, Coastal, Ocean Eng. 146, 04020017. https://doi.org/10.1061/(asce)ww.1943-5460.0000580
Li, Y., Ellingsen, S., 2016. Ship waves on uniform shear current at finite depth: Wave resistance and critical velocity. J. Fluid Mech. 791, 539–567. https://doi.org/10.1017/jfm.2016.20
Li, Y., Smeltzer, B.K., Ellingsen, S., 2019. Transient wave resistance upon a real shear current. Eur. J. Mech. B/Fluids 73, 180–192. https://doi.org/10.1016/j.euromechflu.2017.08.012
Maïssa, P., Rousseaux, G., Stepanyants, Y., 2016. Wave blocking phenomenon of surface

waves on a shear flow with a constant vorticity. Phys. Fluids 28. https://doi.org/10.1063/1.4942116
Maïssa, P., Rousseaux, G., Stepanyants, Y., 2013. Influence of shear-flow vorticity on wave-current interaction. Part 1: Surface gravity waves without surface tension effect.
Markus, D., Hojjat, M., Wüchner, R., Bletzinger, K.U., 2013. A CFD approach to modeling wave-current interaction. Int. J. Offshore Polar Eng. 23, 29–32.
Mucha, P., Deng, G., Gourlay, T., Moctar, O. el, 2016. Validation studies on numerical prediction of ship squat and resistance in shallow water. Proc. 4th MASHCON 83–92. https://doi.org/10.18451/978-3-939230-38-0
Noblesse, F., He, J., Zhu, Y., Hong, L., Zhang, C., Zhu, R., 2014. Why can ship wakes appear narrower than Kelvin's angle ? Eur. J. Mech. B/Fluids 46, 164–171. https://doi.org/10.1016/j.euromechflu.2014.03.012
Peregrine, D.H., 1976. Interaction of water waves and currents. Adv. Appl. Mech. 16, 9–117. https://doi.org/10.1016/S0065-2156(08)70087-5
Roache, P.J., 2016. Verification and Validation in Fluids Engineering: Some Current Issues. J. Fluids Eng. 138, 101205. https://doi.org/10.1115/1.4033979
Salas, M.D., 2006. Some observations on grid convergence. Comput. Fluids 35, 688–692. https://doi.org/10.1016/j.compfluid.2006.01.003
Salas, M.D., Atkins, H.L., 2009. Problems associated with grid convergence of functionals. Comput. Fluid Dyn. 2008 38, 309–314. https://doi.org/10.1016/j.compfluid.2008.01.015
Skop, R.A., 1987. Approximate Dispersion Relation for Wave-Current Interactions. J. Waterw. Port, Coastal, Ocean Eng. 113, 187–195. https://doi.org/10.1061/(asce)0733-950x(1987)113:2(187)
Song, S., Demirel, Y.K., Atlar, M., 2019. An investigation into the effect of biofouling on the ship hydrodynamic characteristics using CFD. Ocean Eng. 175, 122–137. https://doi.org/10.1016/j.oceaneng.2019.01.056
Swan, C., James, R.L., 2000. A simple analytical model for surface water waves on a depth-varying current. Appl. Ocean Res. 22, 331–347. https://doi.org/10.1016/S0141-1187(00)00022-5
Terziev, M., Tezdogan, T., Incecik, A., 2020a. A posteriori error and uncertainty estimation in computational ship hydrodynamics. Ocean Eng. 208, 107434. https://doi.org/10.1016/j.oceaneng.2020.107434
Terziev, M., Tezdogan, T., Incecik, A., 2019. Application of eddy-viscosity turbulence models to problems in ship hydrodynamics. Ships Offshore Struct. 1–24. https://doi.org/10.1080/17445302.2019.1661625
Terziev, M., Zhao, G., Tezdogan, T., Yuan, Z., Incecik, A., 2020b. Virtual Replica of a Towing Tank Experiment to Determine the Kelvin Half-Angle of a Ship in Restricted Water. J. Mar. Sci. Eng. 8, 1–24. https://doi.org/10.3390/jmse8040258
Tezdogan, T., Incecik, A., Turan, O., 2016. A numerical investigation of the squat and resistance of ships advancing through a canal using CFD. J. Mar. Sci. Technol. 21, 86–101. https://doi.org/10.1007/s00773-015-0334-1
Thyng, K.M., Greene, C.A., Hetland, R.D., Zimmerle, H.M., DiMarco, S.F., 2016. True colors of oceanography: Guidelines for effective and accurate colormap selection. Oceanography 29, 9–13. https://doi.org/http://dx.doi.org/10.5670/oceanog.2016.66
Trulsen, K., Mei, C.C., 1993. Double Reflection of Capillary/Gravity Waves by a Non-Uniform Current: A Boundary-Layer Theory. J. Fluid Mech. 251, 239–271. https://doi.org/10.1017/S0022112093003404
Wilcox, D.C., 2006. Turbulence modeling for CFD, 3rd ed, Transportation Research Record. DCW Industries. https://doi.org/10.1016/j.aqpro.2013.07.003
Zhang, J.S., Zhang, Y., Jeng, D.S., Liu, P.L.F., Zhang, C., 2014. Numerical simulation of wave-current interaction using a RANS solver. Ocean Eng. 75, 157–164. https://doi.org/10.1016/j.oceaneng.2013.10.014